STELLAR CO_2 version 2: A database for vibrationally-specific excitation and dissociation rates for Carbon Dioxide

ESA Contract No. 4000118059/16/NL/KML/fg "Standard Kinetic Models for CO_2 Dissociating Flows"

M. Lino da Silva, J. Vargas, and J. Loureiro *

December 21, 2018

Contents

*N-Prime, Instituto de Plasmas e Fusão Nuclear, Instituto Superior Técnico, Av. Rovisco Pais, 1049–001, Lisboa, Portugal

1 Introduction

This short technical report presents version 2 of the STELLAR database update for CO_2, providing a dataset suited for the modeling of vibrationally-specific excitation and dissociation processes in Carbon Dioxide. The implemented datasets provide a better and more physically consistent description of the physical-chemical processes in emerging applications (such as state-to-state modeling of Venus and Mars atmospheric entries, plasma reforming of SynGas, or oxygen production on Mars), as compared to legacy approaches such as the ones based on fist-order perturbation theories (such as the SSH model). The dataset proposed here still makes use of a considerable deal of underlying assumptions and is expected to be superseded in the future by more sophisticated approaches such as Potential Energy surfaces (PES) based trajectory models. However it is expected that this dataset will help improve the accuracy of the state-to-state models developed in the aforementioned applications, and this for a significant amount of time. As PES-based methods are still notoriously complex and difficult to deploy computationally, these are not expected to be widespread before the end of the next decade.

2 Improved Physical Models

The physical models improvements are twofold:

1. A better description for the manifold of vibrational levels for CO_2, extrapolating an accurate low-energy PES by physically-consistent near dissociation potential functions

2. A modeling of the transition probabilities through the Forced Harmonic Oscillator theory, extended for triatomic collinear collisions

2.1 Level energies calculations

We start by defining the asymptotic dissociation limits for the 3 vibration modes of CO_2. These correspond to:

$$\text{Symmetric stretch} \quad CO_2(X^1\Sigma) + 18.53\text{eV} \rightarrow C(^3P) + O(^3P) + O(^1D) \tag{1}$$

$$\text{Bending} \quad CO_2(X^1\Sigma) + 11.45\text{eV} \rightarrow O_2(X^3\Sigma) + C(^3P) \tag{2}$$

$$\text{Asymmetric stretch} \quad CO_2(X^1\Sigma) + \ 7.42\text{eV} \rightarrow CO(X^1\Sigma) + O(^1D) \tag{3}$$

We then selected the Ames-1 PES [1], who has been shown to provide an accurate representation of the CO_2 vibrational levels up to 25,000cm^{-1}. The PES is plotted in the three limits for symmetric stretch (ss), bending (be) and asymmetric stretch (as), and then extrapolated by a repulsive (in the short distance limit) and a Rydberg potential (in the long distance limit), according to the method described in [2]. The radial Schrödinger equation is then solved over the ss and as curves to yield the resulting vibrational levels. In the case of the bending motion, analytical solutions for the corresponding Schrödinger equation exist [3] if the energy dependence of the bending angle follows a specific polynomial expression. For the case of the Ames-1 PES, we find that it is nicely fitted by an $ax^2 + bx^4$ potential, except at angles close to the equilibrium 180° angle. The corresponding analytical solution for the level energies [4] is well behaved (in the sense that it does not have large corrective terms for angles far from the equilibrium, and therefore we might simply extrapolate the values yielded by the Chedin fit [19] up to the bending dissociation limit.

The resulting potential curves (with the vibrational energy levels and wavefunction represented in the case of the ss and as potentials) are presented in Fig. 1.

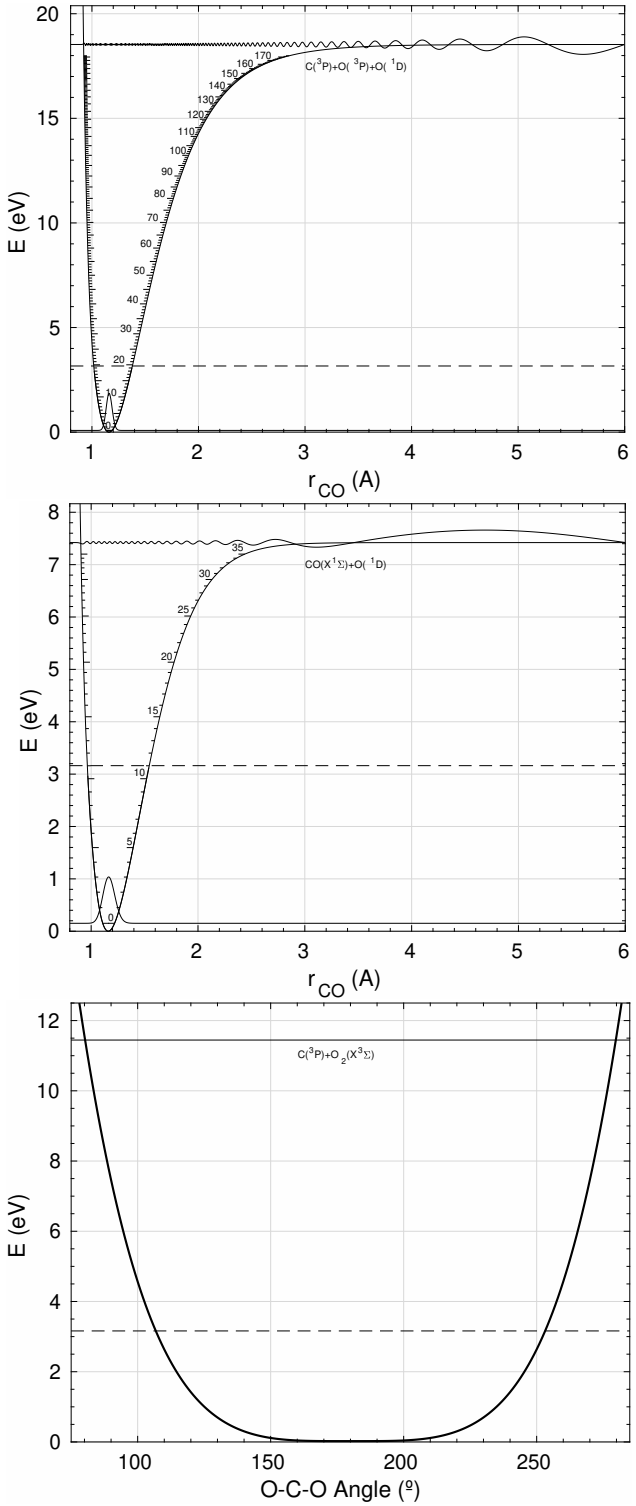

Figure 1: Recalculated potential curves for the CO_2 symmetric stretch, asymmetric stretch, and bending The recalculated level energies, the first and last wavefunctions for the symmetric and asymmetric stretch motions are reported. The dashed line represents the energy limit of 25,000cm^{-1} where the Ames1 PES has been fitted.

2.2 Extension of the FHO theory for triatomic collisions

In this section we detail the underlying theory of the Forced Harmonic Oscillator model, which we have extended for the case of collinear triatomic transitions.

2.2.1 Mass parameters for the three vibrational modes of CO_2

The three vibrational modes of CO_2 (symmetric stretch, asymmetric stretch and bending) have different reduced masses μ for their oscillator movements. These are determined considering the individual molecules displacements and accounting for the conservation of the center of mass in the molecule oscillatory motion [5]. If we further examine the underlying semiclassical theory energy transfer in nonreactive collisions, we notice that we require a further mass parameter γ, which relates the center of mass distance of the colliding particles to the distance between the colliding atoms of both molecules [6]. These are sketched in Fig. 2, where the maximum amplitude of each vibrational movement is represented in full, and the opposite maximum amplitude is represented in faded colors.

The dynamics and amplitude of the displacement coordinates for each of the CO_2 vibrational modes may be determined from a normal modes analysis [7]. For the symmetric stretch, the position of the center of mass doesn't change since each O atom moves in the opposite direction. For the asymmetric stretch, the center of mass doesn't move in the laboratory referential, however in terms of the internal coordinates the center of mass moves between 0.65 and 1-0.65 in a sinusoidal fashion. Since it is the average of the center of mass position that is of interest, this is simply 1/2 of the length of the molecule, just like the symmetric stretch. Identically, for the bending motion, the molecule moves between a minimum angle of α and a maximum of -α, with an average at 180°. This again means that $\gamma = 1/2$ since for an angle α where the center of mass is x, there is an angle $-\alpha$ where the center of mass is $1 - x$

The reduced masses μ, from [5] and the mass parameters γ from this analysis are summarized in Tab. 1.

Table 1: Mass parameters for the three vibrational modes of CO_2

osc. mode	reduced mass μ	mass param. γ
sym. stretch	m_O	1/2
asym. stretch	$\frac{m_C m_O}{m_C + 2m_O}$	1/2
bending	$\frac{m_C m_O}{2(2m_O + m_C)}$	1/2

2.2.2 Outline of the FHO model

Here we summarize the fundamental equations of the FHO model, who yield V–T and V–V–T transition probabilities for any arbitrary collinear, nonreactive collisions for triatomic-triatomic, triatomic-diatomic, and triatomic-atomic pairs.

– V–T transition probabilities [8, 9]:

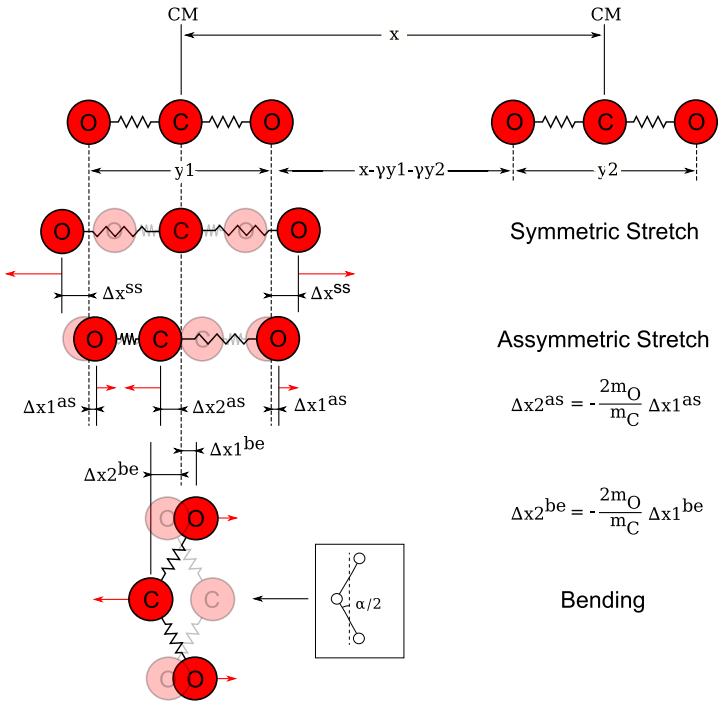

Figure 2: CO_2 mass coordinates for the symmetric stretch, asymmetric stretch and bending modes

$$P(i \to f, \varepsilon) = i!f!\varepsilon^{i+f} \exp(-\varepsilon) \left| \sum_{r=0}^{n} \frac{(-1)^r}{r!(i-r)!(f-r)!\varepsilon^r} \right|^2 \tag{4}$$

with $n = min(i, f)$.

– V–V–T transition probabilities [10]:

$$\begin{aligned} P(i_1, i_2 \to f_1, f_2, \varepsilon, \rho) = & \left| \sum_{g=1}^{n} (-1)^{(i_{12}-g+1)} \right. \\ & \times C_{g,i_2+1}^{i_{12}} C_{g,f_2+1}^{f_{12}} \varepsilon^{\frac{1}{2}(i_{12}+f_{12}-2g+2)} \exp(-\varepsilon/2) \\ & \times \sqrt{(i_{12}-g+1)!(f_{12}-g+1)!} \exp[-i(f_{12}-g+1)\rho] \\ & \left. \times \sum_{l=0}^{n-g} \frac{(-1)^l}{(i_{12}-g+1-l)!(f_{12}-g+1-l)!l!\varepsilon^l} \right|^2 \end{aligned} \tag{5}$$

with $i_{12} = i_1 + i_2$, $f_{12} = f_1 + f_2$ and $n = min(i_1 + i_2 + 1, f_1 + f_2 + 1)$.

ε and ρ are related to the two-state First-Order Perturbation Theory (FOPT) transition probabilities, with $\varepsilon = P_{\mathrm{FOPT}}(1 \to 0)$, $\rho = [4 \cdot P_{\mathrm{FOPT}}(1, 0 \to 0, 1)]^{1/2}$, and C_{ij}^{k} is a transformation matrix calculated according to:

$$C_{ij}^{k} = 2^{-n/2} \binom{k}{i-1}^{-1/2} \binom{k}{j-1}^{1/2} \times \sum_{v=0}^{j-1} (-1)^{v} \binom{k-i+1}{j-v-1} \binom{i-1}{v}. \tag{6}$$

For a Morse intermolecular potential $V(r) \sim E_m(1-\exp(-\alpha r))^2$[1], the expression for ε is given by Cotrell [11], the expression for ρ being identical to the one obtained for a purely repulsive potential [10].

$$\varepsilon = \frac{8\pi^3 \omega \left(\tilde{m}^2/\mu\right) \gamma^2}{\alpha^2 h} \frac{\cosh^2\left[\frac{(1+\phi)\pi\omega}{\alpha\bar{v}}\right]}{\sinh^2\left(\frac{2\pi\omega}{\alpha\bar{v}}\right)} \tag{7}$$

$$\phi = (2/\pi) \tan^{-1} \sqrt{(2E_m/\tilde{m}\bar{v}^2)}$$

$$\rho = 2\left(\tilde{m}^2/\mu\right) \gamma^2 \alpha \bar{v}/\omega. \tag{8}$$

Expressions 4 and 5 have been shown [12] to be cumbersome at high quantum numbers, where limitations with the application of large factorial numbers in the denominator and numerator of the probabilities expressions lead to overflows and underflows that depend on the precision of the floating point operations of the calculating algorithm. These issues may be solved by either a careful tailoring of the simulations with variable precision arithmetics techniques, or the corresponding asymptotic Bessel functions [13] may be used without any noticeable loss of accuracy:

$$P(i \to f, \varepsilon) = J_s^2 \left(2\sqrt{n_s \varepsilon}\right) \tag{9}$$

for $i, f \gg s = |i - f|$, and $n_s = [\max(i, f)! \min(i, f)!]^{-s}$, and

$$P(i_1, i_2 \to f_1, f_2, \varepsilon, \rho) = J_s^2 \left[2\left(n_s^{(1)} n_s^{(2)} \rho_\xi^2/4\right)^{1/2}\right] \tag{10}$$

for $i_1 + i_2 = f_1 + f_2$, and $i_1 + i_2 + f_1 + f_2 \gg s = |i_1 - f_1|$.

Here J_s stands for the Bessel function of the first species and s^{th} order.

The generalizations of the FHO model [14, 15, 16, 12] that allow it to be applied to practical rates calculations are shortly summarized below:

1. Symmetrization of the collision velocity to enforce detailed balance ($\bar{v} = (v_i + v_f)/2$);
2. Accounting for the anharmonicity of the oscillator potential curve using an average frequency $\omega = |(E_i - E_f)/(i - f)|$ if $i \neq f$, and $\omega = |E_{i+1} - E_i|$ if $i = f$;
3. Generalization of the model for nonresonant V–V–T transitions and V–V–T transitions between different species, by replacing $\rho \to \rho \times \xi/\sinh(\xi)$, with $\xi = \pi^2(\omega_1 - \omega_2)/4\alpha\bar{v}$;

[1] We note that if the potential well E_m is set to 0, this reduces to a purely repulsive potential.

4. Generalization of the FHO model to non-collinear collisions (general case) through the multiplication of the parameters ϵ and ρ by steric factors such that $\varepsilon = \varepsilon \times S_{VT}$ and $\rho = \rho \times \sqrt{S_{VV}}$, using the values $S_{VT} = 4/9$ and $S_{VV} = 1/27$, as proposed by Adamovich [14, 16];

5. Modeling vibration-dissociation V–D processes as a transition to a quasi-bound level above the dissociation limit, followed by a decay into the dissociation products [18, 12]: $P(i \rightarrow, \varepsilon) = P(i \rightarrow v_{qbound}, \varepsilon) \cdot P_{decay}$.[2]

One last modification that we propose in this work is a simple semi-empirical correction for the better modeling of near-resonant V–V–T transitions. It is very well-known [14, 24] that the FHO theory fails at predicting these transitions, since it considers a V–V–T process as the product of several V–T processes (e.g. a (0;1)→(1;0) V–V–T transition will be treated as a sequence of two V–T transitions: (0;1)→(0;0)→(1;0)), which implies artificially larger energy jumps and in consequence an underestimation for the transition probability. The simple semiempirical correction of Fig. 3 is carried out.

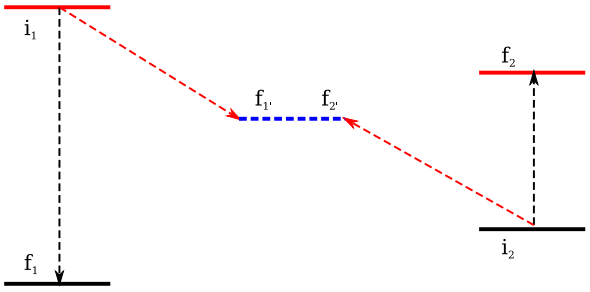

Figure 3: Forced Harmonic Oscillator correction for near-resonant V–V–T transitions

A more adequate transition probability is obtained in for the purposes of calculating the transition probability, if we consider a transition of both initial states to a fictitious state such that $|\Delta E_{(i_1 - f_1')}| = |\Delta E_{(i_2 - f_2')}| = |\Delta E_{VVT}|/2$

3 Results

We consider the vibrational levels list obtained in section 2.1, which yields respectively 240 v_1, 128 v_2, and 42 v_3 levels up to their respective dissociation limits.

The procedure employed for the fitting of the experimental data is to consider the aforementioned level energies, and to iteratively determine the set of intermolecular Morse potential parameters α^{-1} (repulsive potential parameter and E bottom of the Morse potential for long range attractive forces. Further, we iteratively determine the S_{VT} steric coefficient for V–T transitions, and the S_{VVT} steric coefficient for V–V–T transitions.

In this first version of the database, the determined rates are based whenever possible on data where the collisional partner is CO_2. Data derived from collisions with other collisional partners is only taken into account if data for CO_2–CO_2 collisions is absent. We therefore assume that $K_{CO_2-X} = K_{CO_2-CO_2}$.

[2] with $P_{decay} \sim 1$

3.1 Short review of measured and calculated intermolecular potentials

The approach that has been followed in the past [24] is to consider the α^{-1} and E_m parameters as fully adjustable, iterating the values until a best fit with reference rates (either experimental or from high-fidelity numerical models) is achieved. With this said, a review of the available data on intermolecular potentials is always pertinent, since it allows establishing some boundaries allowing the verification of the iteratively determined isotropic Morse potential. It is also useful for determining the ratios of given state-specific potentials for different collisional pairs, allowing the extension of a calculated state-specific dataset to another one (for example, extending a dataset for CO_2–CO_2 collisions to CO_2–N_2 collisions).

Here we have investigated molecular beam experiments that allow the determination of short-range repulsive potentials, and "ab-initio" multidimensional intermolecular PES that are used in high-fidelity trajectory methods for the determination of synthetic transition rates (quasiclassical or full quantum methods).

Leonas [25] has carried out an extensive study of the repulsive intermolecular forces between a large number of atomic, diatomic and triatomic species pairs. The results for the chemical species relevant to CO_2–N_2 gas mixtures are summarized in Tab. 2.

Table 2: Measured repulsive potentials from Ref. [25]

System	A (keV)	α^{-1} (Å^{-1})	A (keV)	α^{-1} (Å^{-1})
O - CO_2	1	4.06	7	3.89
N_2 - CO_2	1.17	4.06	30	3.78
O_2 - CO_2	0.49	3.58	8.72	3.33
CO - CO_2	0.897	3.81	19.2	3.55
CO_2 - CO_2	1.09	3.96	44.9	3.43

We complement this analysis with a review of the PES from Bock [26] for CO_2–CO_2 collisions, which is easily reproducible based on the expressions published therein. Fig. 4 presents the intermolecular potential for the different molecular orientations.

Each collision configuration has been fitted to a Morse potential. The corresponding repulsive and well depth parameters are reported in Tab. 3.

Table 3: Morse fit to the Bock potential [26] for different collision configurations

Configuration	E (K)	α^{-1} (Å^{-1})
T	616	4.87
Linear (– –)	75	5.46
X	193	4.89
Slip parallel (//)	642	4.56

These two sets of data may then be considered as a reference regarding intermolecular potentials. Any iteratively determined potential should be expected to remain close to these values.

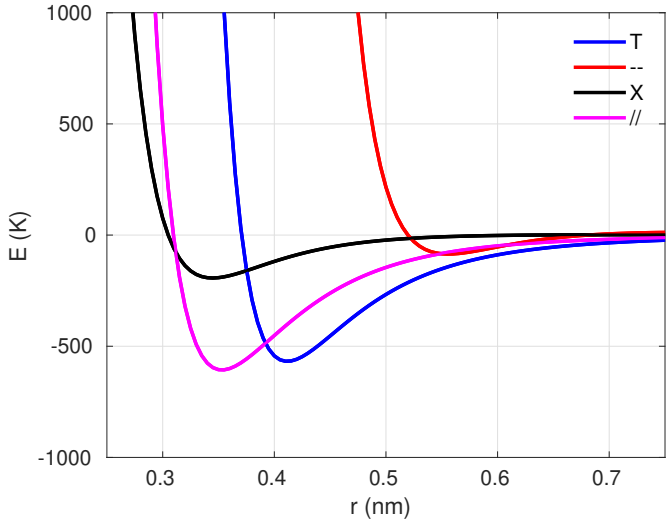

Figure 4: Bock intermolecular potential [26] for different collision geometries

3.2 v_2 V–T rates determination

The procedure for the determination of a dataset of v_2 V–T rates is rather straightforward, since Blauer [27] proposed a set of rates

$$CO_2(0, v_2, 0) + CO_2 \rightarrow CO_2(0, v_2 - 1, 0) + CO_2 \tag{11}$$

for v_2=[5–1], from room temperature up to 3,000K. A best fit between the FHO model and the Blauer data is found for the intermolecular parameters from Tab. 4. A comparison of Blauer's rates with the best-fit FHO rates is presented in Fig. 5

Table 4: Best-fit intermolecular potential and steric factor parameter

α^{-1}(Å^{-1})	E(K)	S_{VT}
4.3	650	6×10^{-4}

3.3 v_1 and v_3 V–T rates determination

The procedure for the calculation of v_1 and v_3 V–T rates is significantly more complex and requires a significant number of underlying assumptions. These rates have to be considered as a "best-guess" estimation since pure V–T quenching rates are found to be too low to be accurately determined in experimental measurements [28], and since detailed PES-based simulations are lacking for these modes[3].

Here we start by considering the measurements compiled by Byriukov [29] for the total quenching rate of $CO_2(v_3)$:

$$CO_2(0, 0, v_3) + CO_2 \rightarrow CO_2(n, m, 0) + CO_2 \tag{12}$$

[3]also since the pure V–T rates for modes v_1 and v_3 have low transition probabilities, they are difficult to determine with enough accuracy, unless an inordinate number of trajectories is sampled using PES models

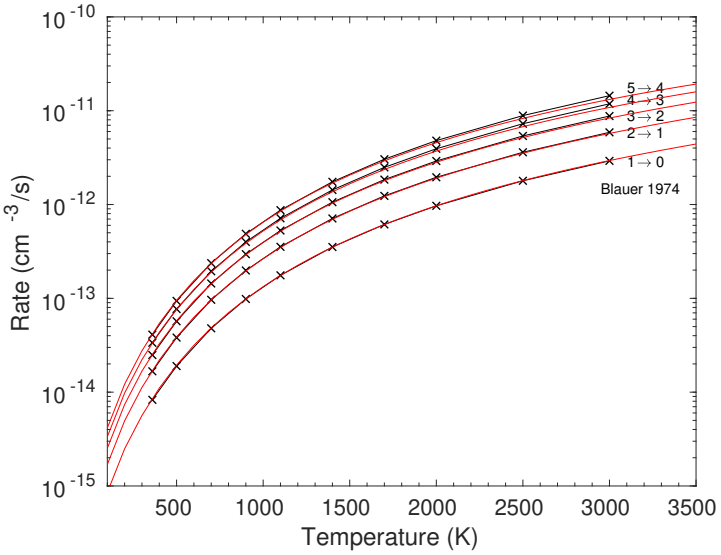

Figure 5: Comparison of Blauer [27] rates (–x–) with rates from the FHO model (–)

We do a best-fit of this rate using the FHO model. The corresponding intermolecular parameters are presented in Tab. 5. A comparison of the experimental data with the best-fit FHO rate is presented in Fig. 6.

Table 5: Best-fit intermolecular potential and steric factor parameter

$\alpha^{-1}(\text{Å}^{-1})$	E(K)	S_{VT}
7	1700	1/3

We notice thet the best-fit potential differs significantly from the boundaries recommended in section 3.1. This is not surprising as the quenching rate is in fact a mix of different transitions to several intermode levels below the (001) level.

Losev carried out a review [28] of the temperature-dependent. branching ratios for the $CO_2(v_3)$ quenching rate. We divide our global FHO quenching rate (Fig. 6) by the branching ratios proposed in the T=300–2000K range and obtain the set of arrhenius rates[4] presented in Tab. 6. The corresponding rates (original and fitted to an Arrhenius expression) are presented in Fig. 7. The Arrhenius fit extrapolates well in the low-temperature range, and in the high-temperature range (remaining below the gas-kinetic rate up to 10,000K and beyond).

This is insufficient to provide any estimate of the v_3 VT deactivation rate $CO_2(00^01) \rightarrow CO_2(00^00)$, and it is necessary to review other works in search for data that might complement these results.

A bibliography research yields PES trajectory data from Billing [22], where the calculations (according to the VVC IOS method[5]) did not have enough trajectories sampled to yield a reliable rate. Schatz [30] reported a v_3 excitation cross-section below $2 times 10^{-18} \text{cm}^3$ for CO_2–O collisions. Clary [31] carried out PES-based simulations (VVC IOS method) for collisions with noble gas atoms (He, Ne, Ar), however its

[4] after performing a fit to an Arrhenius expression
[5] vibrational close-coupling rotational infinite order sudden

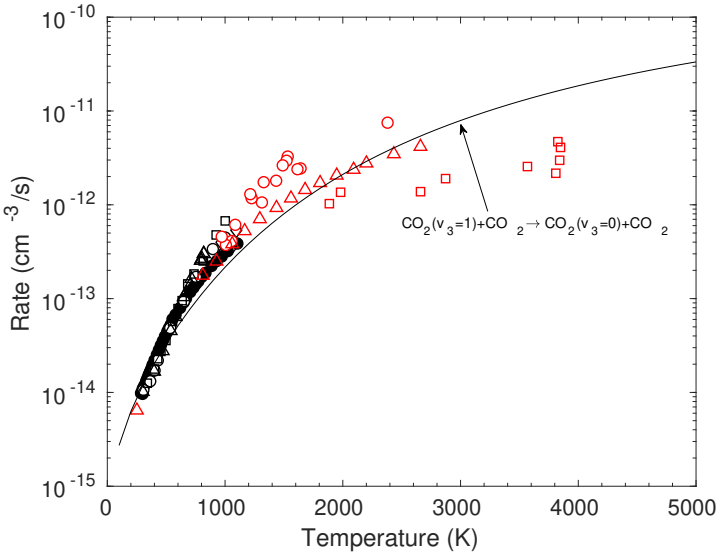

Figure 6: Comparison of Byriukov [29] rates (points) with best-fit from the FHO model (–)

Table 6: Arrhenius – $AT^n \exp(-\theta_r/T)$ – rate expressions for v_3 quenching rates, T=[300–2,000]K

Transition	A	n	θ_r
$00^01 \rightarrow 02^00 + 10^00$	7.93×10^{-19}	1.74	156
$00^01 \rightarrow 03^10 + 11^10$	1.82×10^{-21}	2.83	1788
$00^01 \rightarrow 04^00 + 12^00 + 20^00$	4.29×10^{-13}	-0.36	1469
$00^01 \rightarrow 01^10$	5.04×10^{-21}	2.54	4607

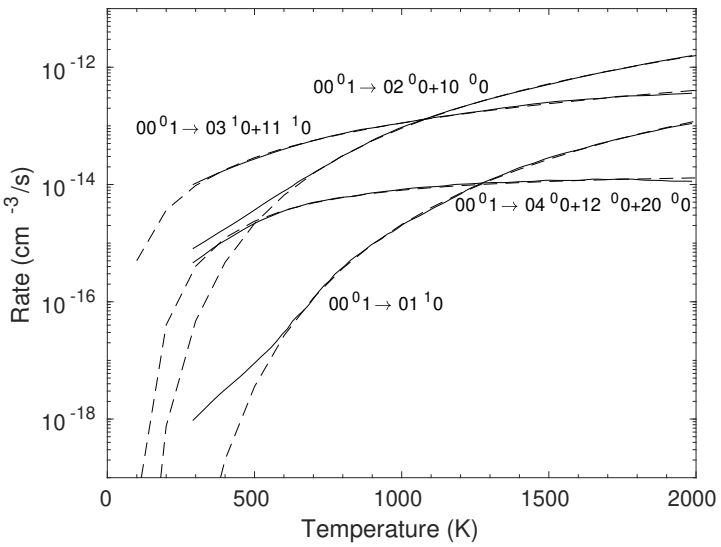

Figure 7: Quenching rates in the 300–2000K range, assuming the branching ratios proposed by Losev [28]. The corresponding Arrhenius fits are presented in dashed lines

results are limited in range (around 300K), lack transitions to the v_3 state, and are difficult to transpose to CO_2–CO_2 collisions. Chu [32] presented an experimentally measured set of transition probabilities for CO_2–H collisions at two different temperatures (18,000 and 24,000K). Again his results are difficult to transpose for the case of CO_2–CO_2 collisions. Nevertheless, we may summarize these results to have a clearer view on the influence of the mass of the colliding partner in the transfer rates for the different vibrational modes. This is done in Tab. 7.

Table 7: Probabilities for T–V excitation processes for CO_2–X collisions

	H(18–24kK)[1]	He(300K)[2]	Ne(300K)[2]	Ne(300K)[3]	Ar(300K)[2]	O(2–6eV)[4]
$P_{0\to v_1}$	12–16%	1.8e-5	1.6e-7	4.0e-7	4.9e-6	
$P_{0\to v_2}$	16–21%	0.93%	0.16%	0.16%	0.12%	
$P_{0\to v_3}$	1.1–1.7%	5.9e-9	4.4e-7	–	–	<0.05%

[1]: Chu 1983 [32]; [2]: Clary 1981 [31]; [3]: Billing 1981 [22]; [4]: Schatz 1981 [30]

One should further note that Siddles [33] reviewed the dependence on the collisional partner for the quenching ratios of the v_3 and v_2 levels. These are reported in Tab. 8

Table 8: Quenching ratio v_3/v_2 dependence on the collisional partner

	155K	295K
H_2	0.004	0.020
D_2	0.010	0.013
He	0.028	0.018
Ne	0.65	0.37
N_2	1.7	1.0
O_2	2.5	0.81
Ar	4.7	2.1
CO_2	4.0	1.8
Xe	5.7	7.2

Ultimately, we considered the results of Harvey [34], who used a VCC IOS method to obtain energy-dependent transitions cross-sections for the excitation of the v_1, v_2, v_3 modes from the ground-state of CO_2, for an energy range of 1–6eV, and considering a CO_2–O collision. This work has been carried out in relation of the investigation for the energy transfer process:

$$CO_2(01^10) + O \to CO_2(00^00) + O \tag{13}$$

which is known to be of paramount importance for upper-atmospheric processes [35].

The excitation cross-sections have been carefully extrapolated in the lower range and converted into de-excitation cross-sections using the detailed balance principle. A comparison has then been carried out between these cross-sections, and the v_2 quenching cross-section calculated at low collision energy by Lara–Castells [36], which accounted for spin-orbit interactions of the 3 different electronic states for the O atom, something that is neglected in the calculations of Harvey. The obtained probabilities are presented in Fig. 8

We see that the cross-sections for the v_2 excitation process, as proposed by Harvey, are underestimated in the low-energy limit, likely due for the model not accounting for spin-orbit interactions. Lara–Castells

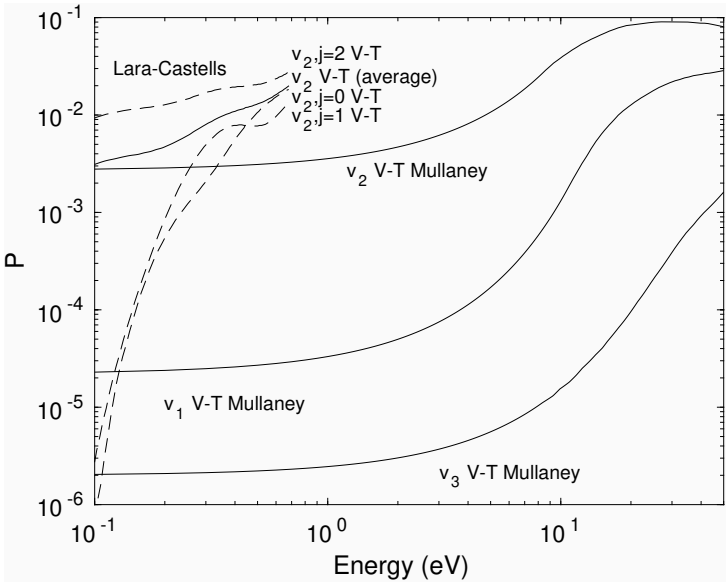

Figure 8: Quenching (1–0) probabilities for the v_1, v_2, v_3 modes, as proposed by Harvey [34], and comparison with the probabilities obtained by Lara–Castells for the v_2 mode quenching

shows that the collision CO_2+O($^3P_2$) has significantly higher probabilities, as a consequence of spin-orbit interactions, therefore yielding a much higher transition cross-section at low impact energies, which helps explaining the abnormally high transition rate for the process of Eq. 13 at lower temperatures. Despite this, the results from Harvey and Lara–Castells are not significantly different, and we may convert the resulting de-excitation probabilities from Harvey to yield the corresponding rates. Then we may further compare the resulting rates with other v_2 de-excitation data. This is presented in Fig. 9.

The comparison with Castle [37] data in the low-temperature range (142–490K), and with with Center [38] in the high-temperature range (2,000–4,000K) yields a satisfactory comparison in terms of orders of magnitude, despite that the low-temperature rates are one order of magnitude higher and show the well-known inverse temperature dependence [35], due to the CO_2+O($^3P_2$) spin-orbit interaction [36]. Further, the rate derived from Harvey's cross-sections appears to be relatively "flat" at higher temperatures, despite evidences of increase in the transition rates, as shown by Center's data. For reference, Blauer's proposed rate for $CO_2(v_2)$–CO_2 quenching is also reported.

In conclusion, and despite the shortcomings from the rates that are derived from Harvey's extrapolated cross-sections, these are considered to be credible enough for the purposes of this work, which are not to directly deploy these in kinetic models, but instead to investigate the 0–1 quenching rates ratios between the v_1, v_2, v_3 modes, for a large temperature range. These are reported in Fig. 10.

The ratios between the v_2 and v_3 1–0 de-excitation rates remain relatively insensitive to temperature, ranging from 7.4×10^{-4} at 2,000K and 6.4×10^{-4} at 10,000K respectively. A similar trend is found for the v_3/v_1 ratio, who varies from 0.09 to 0.06 in the same temperature range. This may be compared to the estimations proposed by different author. Moore [39] cites a probability of 10^{-10} at room temperature, comparable to that for N_2 or CO relaxation. Since the v_2 relaxation probability is 3×10^{-5}, this yields a v_2/v_3 ratio of 3×10^5. Fridman ([40], pp. 270, Fig. 5–13) proposes a v_3 1–0 rate of 10^{-17} at room temperature. This corresponds to a v_2/v_3 ratio of about 10^3, since the v_2 relaxation rate is about 10^{-14}.

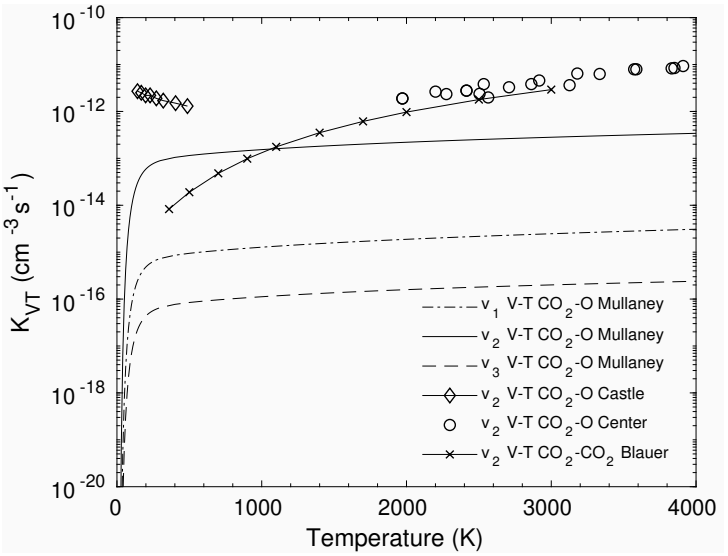

Figure 9: Quenching (1–0) rates the v_1, v_2, v_3 modes, as proposed by Harvey [34], and comparison with other reported data for the v_2 mode

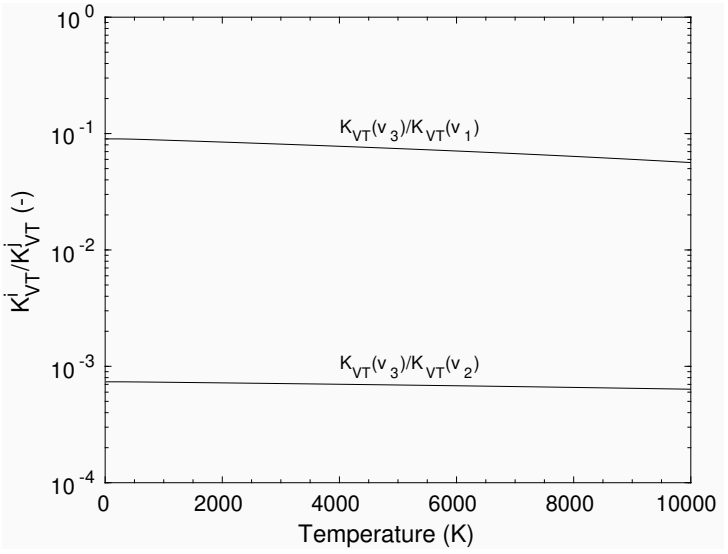

Figure 10: Quenching (1–0) rate ratios between the v_1, v_2, v_3 modes, from the cross-sections proposed by Harvey [34]

Kustova [41] and Armenise [42] present VT relaxation rates for v_1, v_2 and v_3. The v_3/v_2 ratio ranges from 10^{-8} at 700K to 10^{-5} at 2,000K[6] for the former, and from 10^{-8} at 1000K to 10^{-4} at 4,000K for the latter.

Overall, the v_2/v_3 ratio obtained in this work appears quite reasonable given the scattering of the estimations from other authors.

For the v_3/v_1 rate ratio we may simply compare this result to the one obtained by considering an identical intermolecular potential for both modes (a reasonable assumption, regarding the kinematic similarity between both symmetric and asymmetric stretch motions) and obtaining the corresponding 1–0 de-excitation rates, whose ratio will depend only from the respective energy spacings (the v_1 rate being higher due to the lower energy jumps). Using the intermolecular potential from 5 we obtain 0.07 at 2,000K and 0.5 at 10,000K. The latter value is one order of magnitude above the ratio from Harvey, which is not surprising since – as discussed before – this intermolecular potential is rather unrealistic. If we use a more reasonable potential such as the one from 4, we obtain 0.005 at 2,000K and 0.09 at 10,000K. Here the ratio at lower temperature is one order of magnitude below the ratio from Harvey, but the high-temperature limit is relatively close to the value from the ratio of the rates based on Harvey's cross-sections.

The knowledge of the 1–0 rate ratios now allow-us to determine the v_3 1–0 de-excitation rate. We do not consider the fitted potential from Tab. 5, in view of the aforementioned issues. Instead we use the potential for v_2 de-excitation as a basis (Tab. 4) since it has good agreement with the review of section 3.1 and since it is expected the the intermolecular potentials for the stretching and bending motion shouldn't be intrinsically different.

Keeping the intermolecular potentials and steric factors of Tab. 4, we obtain the corresponding v_3 and v_1 rates, that we may compare to the ratios for the rates issued from Harvey:

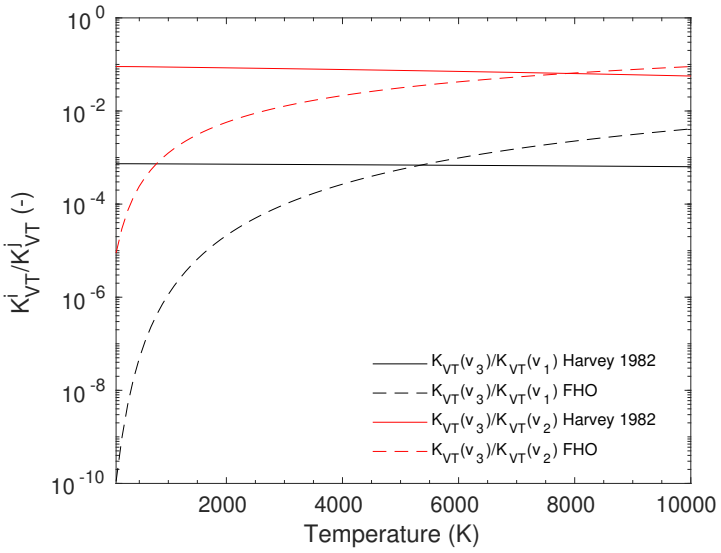

Figure 11: Same as Fig. 10, with the ratios for the V_1, v_2, v_3 FHO rates using the potential parameters of Tab. 4

Unlike Harvey's rate ratios, the FHO rate ratios evidence a significant variability over the temperature

[6] and a v_1/v_2 ratio ranging from 10^{-4} to 10^{-2} in the same temperature range

range, and are relatively consistent with the rate ratios proposed from different literature sources[7]. Nevertheless, the average values for the ratios are relatively consistent in terms of orders of magnitude, for the temperature ranges where V–T processes will be noticeable. When calculating v_1 and v_3 FHO rate coefficients, we then opt for considering the exact same intermolecular potential than for v_2 V–T rates (Tab. 4).

3.4 On the question of the Fermi resonance modeling

It is very well known that the v_1 and v_2 levels are coupled through a Fermi resonance. Indeed the harmonic oscillator frequencies are respectively 1335.8cm^{-1} for the v_1 mode and 667.2cm^{-1} for the v_2 mode. This leads to an energy difference in the fundamentals of about 1.5cm^{-1}, however, the resonance energy shifts lead to a perturbed level energies difference of 102cm^{-1}:

$$CO_2(10^00) + M \leftrightarrow CO_2(02^00) + M + 102\text{cm}^{-1} \tag{14}$$

The exchange rates will be near-resonant and will have considerable high probabilities. Upper and lower bounds for the Fermi transition rate for the first resonance pair (1000↔0200) have been proposed by Eckermann [44], which corresponds to a probability between 11.1–13.4%. This has been put to use in most of the proposed CO_2 vibrational models (see for example [40, 43]) since it becomes a convenient way to lump the v_1 and v_2 degrees of freedom into a v_{12} level, therefore decreasing the complexity of simulation approaches.

Nevertheless, consistent experimental accounts show that the Fermi resonance is often insufficient to keep corresponding v_1 and v_2 levels in equilibrium, since other near-resonant transitions will often selectively deplete the v_1 or v_2 levels [45, 28, 46, 47, 48]. More importantly, due to the anharmonicity of the v_1 potential curve, the Fermi resonance will not extend very far up into the vibrational ladder. Using the expression from Chedin [19], the energy resonances for the Fermi levels ($v_1 \leftrightarrow v_2 = 2v_1$) will be, respectively 1.49cm^{-1}, 10.62cm^{-1}, 27.66cm^{-1}, 52.86cm^{-1}and 86.48cm^{-1} for v_1=1–5. Clearly the Fermi resonance only occurs for the very first v_1=1–3 levels, since resonance energies are typically below 20–30cm^{-1} [21]. Therefore, all the models that are assuming a Fermi coupling between the v_1 and v_2 levels up to the dissociation limit are grossly extrapolating the validity range for this resonance.

It is also worthy to note that there are many other kind of possible resonances in CO_2. For example Finzi [49] measured ubiquitous V–V equilibration processes of the type:

$$CO_2(10^01) + CO_2(00^00) \rightarrow CO_2(10^00) + CO_2(00^01) - 22\text{cm}^{-1} \tag{15}$$

$$CO_2(02^01) + CO_2(00^00) \rightarrow CO_2(02^00) + CO_2(00^01) - 21\text{cm}^{-1} \tag{16}$$

these processes have been found experimentally to have the cross-sections of 24Å^2 and 21Å^2 respectively. Since the collisional cross-section for the CO_2–CO_2 pair is 48.8Å (calculated accounting for the species radius in Svehla's compilation [50]), this corresponds to a transition probability of 49% and 41% respectively. Nevertheless, since we are in the approach of considering complete separability of the different CO_2 modes, these rates do not provide any redistribution of the level populations and may be ignored.

[7] although the SSH-based works will inevitably yield similar rate ratio dependences since the SSH theory is a first-order approximation of the FHO theory

3.4.1 Accounting for accidental resonances

The large number of vibrational levels present in the CO_2 molecule make it important to check whether any arbitrary levels are in resonance (which we will label here as "accidental" resonances). We consider a limit of about 25cm^{-1}, which is about 10% of the available thermal energy (k_BT) at room temperature. For any resonance below this value, we consider the transition probability to amount to the same value than for the (1000↔0200) Fermi resonance, which is P=12%. Considering the CO_2–CO_2 hard-sphere collisional cross-section $\sigma = 48.8$Å, and assuming that the transition probability is T independent, we get the corresponding rates for these resonant transitions:

$$K_{res}(T) = P\sigma\left(\frac{8k_BT}{\pi\mu}\right)^{1/2} = 1.82\times10^{-11}T^{1/2} \tag{17}$$

where μ is the CO_2 collision pair reduced mass.

We further chose to account for a set of additional near-resonant rates in the 25–100cm^{-1} range. We consider the classical Landau-Teller model to estimate these from the single-quantum transition rate K_{10} [51, 52]:

$$K_{10} \sim \exp\left\{\left[-\frac{54\pi^2\mu x_0^2(\Delta E_v)^2}{h^2k_BT}\right]^{1/3}\right\} \tag{18}$$

where x_0 is the radius of interaction between the colliding species.

This expression simplifies to $K_{10} \sim \exp\left\{\left[-0.013x_0^2(\Delta E_v)^2/T\right]^{1/3}\right\}$ with x_0 in Å and $(\Delta E_v)^2$ in cm^{-1}. This further reduces to $K_{10} \sim \exp\left\{\left[(\Delta E_v)^2/T\right]^{1/3}\right\}$ considering that typical values of x_0 are in the range of 0.5–1.5Å [52].

We then normalize the rate K_{10} to the one from eq. 17, considering a ΔE_v=25cm^{-1}, and T=300K: $K_{10} \simeq 0.5$ and $K_{res} = 3.14\times10^{-11}$. We then have the near-resonance rate K'_{res}:

$$K'_{res}(T, \Delta E_v[\text{cm}^{-1}]) = 1.57\times10^{-11}\exp\left\{\left[-\frac{(\Delta E_v)^2}{T}\right]^{1/3}\right\} \tag{19}$$

The determined CO_2 resonant levels are listed in appendix A, along with the energy corresponding differences, which allow calculating the corresponding transition rates according to Eq. 17 if the energy mismatch is lower than 25cm^{-1}, or Eq. 18 if the energy mismatch is between 25 and 100cm^{-1}.

3.5 v_1, v_2, and v_3 V–V–T rates determination

Owing to the hypothesized importance of ladder-climbing V–V–T phenomena in CO_2 dissociation processes, we have chosen to extend our analysis to the modeling of these aforementioned processes. Our analysis focuses on the monoquantum processes which are expected to be near resonant for a large range of the vibrational ladder

$$CO_2(v_k = i) + CO_2(v_k = i) \rightarrow CO_2(v_k = i+1) + CO_2(v_k = i-1) + \Delta E, \tag{20}$$

where v_k is any of the vibrational modes v_1, v_2, or v_3.

We first examine the degree of near-resonance for the processes above. We compare the energy defects for those transitions from the extrapolated potentials determined in section 2.1 (full lines), with the ones obtained using Chedin's expression [19]. The results are reported in Fig. 12.

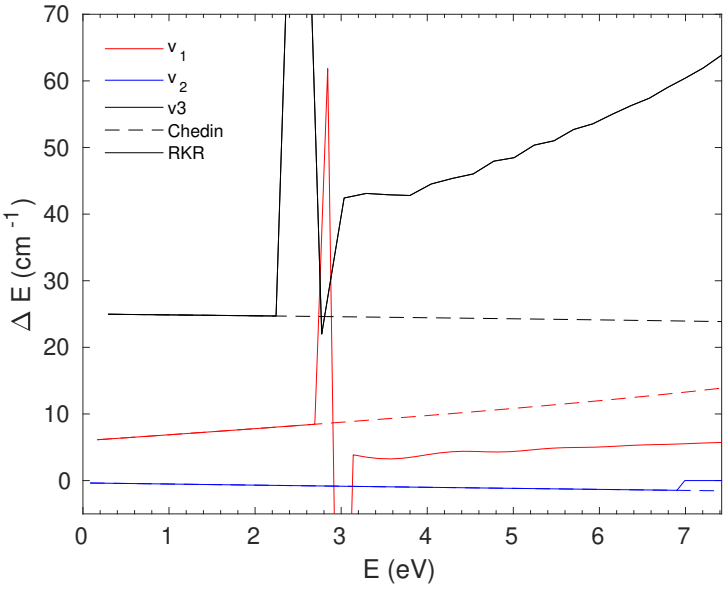

Figure 12: Energy defects for the monoquantum transition of Eq. 20

As expected, the results from the NASA Ames potential [1] and Chedin's expression [19] coincide up to the limits where the AMES potential is considered to no longer be accurate and starts being extrapolated by an adequate near-dissociation potential. Since we switch from the Chedin expression to the radial Schrödinger equation solutions without any special care in maintaining first and second order derivatives continuity, there is a discontinuity at the quantum levels where this occurs. This might be revisited in future versions of the database if it is found to impact the modeling of CO_2 excitation and dissociation processes adversely.

From a further analysis of the calculated energy defects, we notice that all the V–V–T rates will be near-resonant up to the 7.42eV dissociation limit, with v_1 having a maximum energy defect of about 10cm^{-1}, v_2 an energy defect of about 1–2cm^{-1}, and v_3 an energy defect of about 60cm^{-1}. This means that the V–V–T transition rates for all the 3 vibrational modes are expected to be quite high.

We firstly examine the v_3 mode. Experimental data is scarce and limited to the near-resonant (25cm^{-1} energy defect) $CO_2(001)+CO_2(001)\rightarrow CO_2(000)+CO_2(002)$ [53, 54]. A fit to the FHO theory has proved to be unfeasible given the very high transition probabilities reported in these references. Actually, these exceed one for the rate at 700K proposed by Thomason [54]. The comparison between the experimental rates, the closest FHO rate, and the gas-kinetic rate are presented in Fig. 13.

As the experimental data is puzzling, and owing to the questions regarding its comparison with the gas-kinetic rate, we have decided against using it for calibrating the FHO potentials for V–V–T transitions. Instead we have reviewed the near-resonant CO_2–N_2 "laser" transition $CO_2(001)+N_2(0)\rightarrow CO_2(000)+N_2(1)$ for which an extensive amount of data exists [39, 55, 56, 57, 27, 20]. A best-fit for the FHO theory, including the near-resonant V–V–T trasitions correction, is presented in Fig. 14.

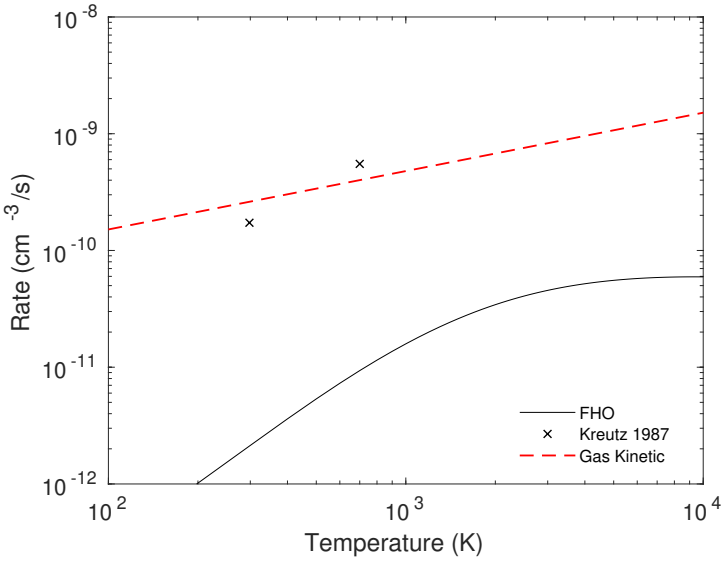

Figure 13: Comparisons for the $CO_2(001)+CO_2(001)\rightarrow CO_2(000)+CO_2(002)$ V–V–T rate

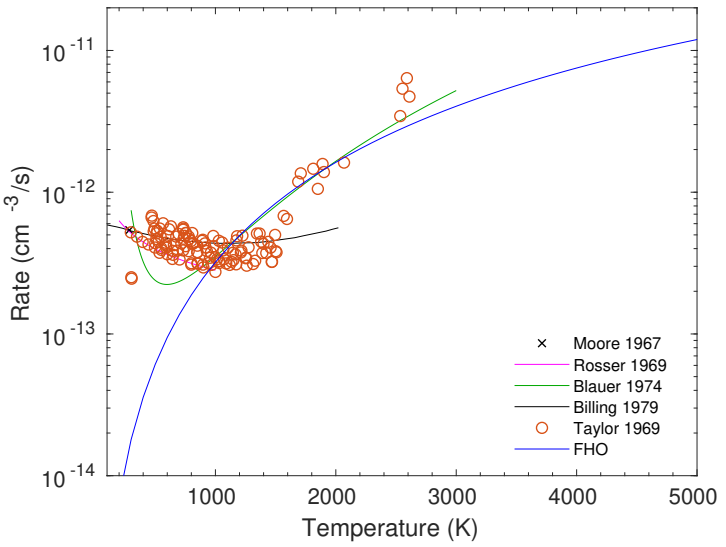

Figure 14: Comparisons for the $CO_2(001)+N_2(0)\rightarrow CO_2(000)+N_2(1)$ V–V–T rate

The FHO theory, with the correction for near-resonant V–V–T transitions, is found to provide a good agreement with available experimental data in the high-temperature limit. For Low temperatures, it is necessary to resort to the Sharma–Brau theory [21]. This may be simply done through adding this rate to the FHO rate since both are mutually exclusive (Sharma-Blau theory gives a negligible rate at high temperatures, and the FHO theory at low temperatures).

The steric factors for the best fit are presented in Tab. 9. The intermolecular potential parameter is kept at the same value than for the V–T transitions case (see Tab. 4).

Table 9: Best-fit steric factor parameters for the $CO_2(001)+N_2(0)\rightarrow CO_2(000)+N_2(1)$ V–V–T rate

S_{VT}	S_{VVT}
6.5×10^{-5}	6.5×10^{-5}

An additional comparison is carried against a review of measured $CO_2(001)+CO(0)\rightarrow CO_2(000)+CO(1)$ V–V–T rates, published by Miller [58]. This is presented in Fig. 15. Again, a best-fit is obtained for the intermolecular potential of Tab. 4, with a slight adjustment of the V–T steric factor S_{VT}. The result for the "standard" $S_{VT} = 6\times10^{-4}$ is also reported, and it could be argued that this is also a reasonable fit, owing to the scattering for the experimental data. As for all the near-resonant V–V–T transitions, these are found to be insensitive to the V–V–T steric factor S_{VVT}, who is set by default equal to S_{VT}.

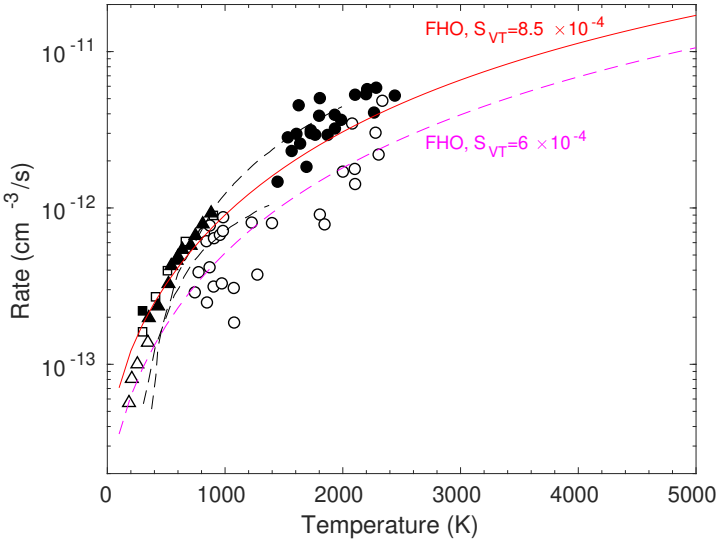

Figure 15: Comparisons for the $CO_2(001)+CO(0)\rightarrow CO_2(000)+CO(1)$ V–V–T rate

We conclude our analysis for the V–V–T rates with a comparison against the CO_2–CO_2 v_2 bending rates published by Blauer [27]. A select number of published V–V–T rates is tested against not only our FHO model, but also our proposed Landau–Teller rate for CO_2–CO_2 near resonant rates (Eq. 18. The comparison for the $CO_2(03^30)+CO_2(01^10)\rightarrow CO_2(02^20)+CO_2(02^20)$ V–V–T rate is presented in Fig. 16.

The steric factor had to be adjusted to $S_{VT} = 1.7\times10^{-6}$, but other intermolecular parameters were

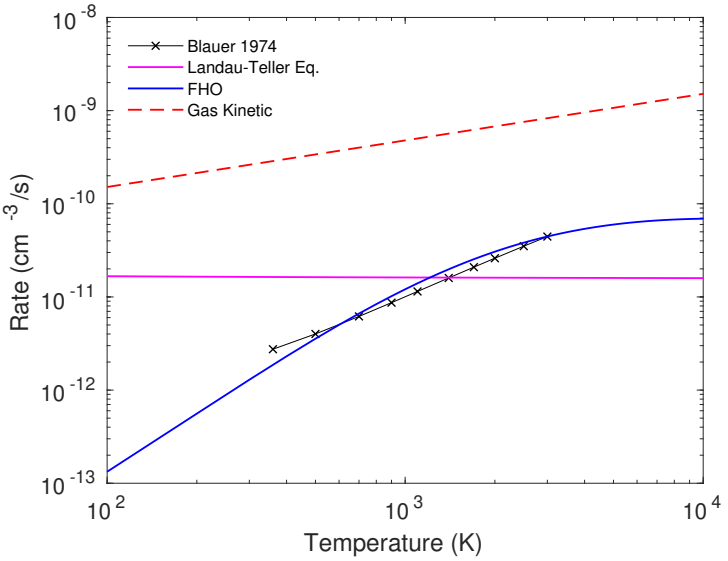

Figure 16: Comparisons for the $CO_2(03^30)$+$CO_2(01^10)$→$CO_2(02^20)$+$CO_2(02^20)$ V–V–T rate

kept the same as in Tab. 4. The comparison with the FHO theory provides a reasonable agreement with the published Blauer rates, while the Landau–Teller equation will only yield the correct order of magnitude, being flat over the whole temperature range. This is to be expected in the scope of Eq. 18, since the energy defect for this transition is only ΔE =0.5cm^{-1}.

A further set of v_2 V–V–T rates has been fitted in the same fashion, with the previous rate reproduced alongside two more. The considered transitions are then:

$$CO_2(03^30) + CO_2(01^10) \rightarrow CO_2(02^20) + CO_2(02^20) \quad (21)$$
$$CO_2(04^40) + CO_2(00^00) \rightarrow CO_2(03^30) + CO_2(01^10) \quad (22)$$
$$CO_2(04^40) + CO_2(02^20) \rightarrow CO_2(03^30) + CO_2(03^30) \quad (23)$$

The comparison with Blauer rates is presented in Fig. 17. In this case, the intermolecular potential parameters are once more kept he same as in Tab. 4, however the V–T steric factors S_{VT} had to be considerably adjusted. The best-fit were respectively $S_{VT} = 1.7 \times 10^{-6}$, 6.0×10^{-6}, and 0.1×10^{-6}. Again, the S_{VVT} steric factors were insensitive for this kind of almost resonant rates.

3.6 Production of complete V–T datasets and V–V–T

Based on the FHO parameters determined in sections 3.2 and 3.3, rate datasets for v_1, v_2, v_3 V–T transitions have been determined in the T=[100–100,000K] range. v_1, v_2, v_3 V–V–T transitions. $((i;f) \rightarrow (i-1;f+1))$ have been determined in the same temperature range. The intermolecular parameters have been kept constant to those from Tab. 4 with $S_{VVT} = S_{VT}$, owing to the conclusions from Sections 3.2,3.3, and 3.5. For the case of the v_2 and v_3[8] near-resonant V–V–T transitions, we have found that V–T S_{VT} steric factor values below the nominal value of 6×10^{-4} had to be considered for best-fit practices. Nevertheless, we ended up considering the nominal value for all CO_2–CO_2

[8]for the "laser" CO_2–N_2 transition

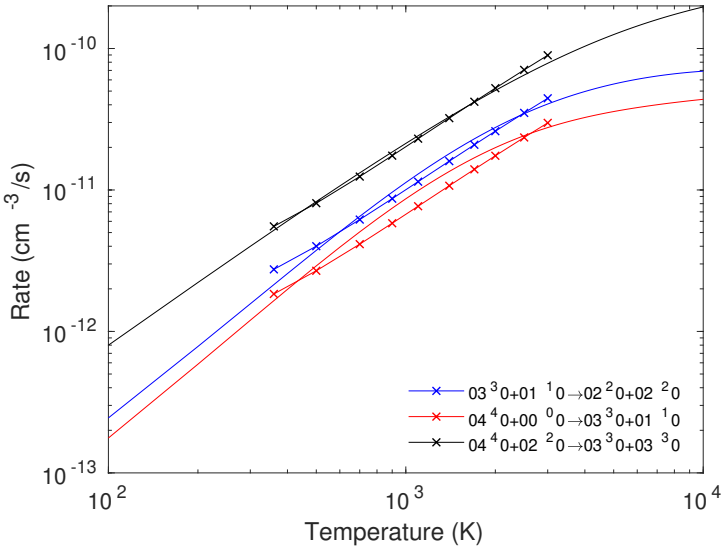

Figure 17: Comparisons for the $CO_2(v_2)$ V–V–T rates from Eqs. 21 to 23

V–V–T transitions since this value is appropriate for the $CO_2(001)+CO(0)\rightarrow CO_2(000)+CO(1)$ V–V–T transition that should be by analogy the physically closest one to a CO_2–CO_2 V–V–T transition. This assumption may nevertheless be revisited in future revisions of the database.

We have defined as a cutoff energy the dissociation energy for the asymmetric mode stretch of $CO_2(X^1\Sigma)$ at 7.42eV. This yields v_1^{max}=50, v_2^{max}=85, and v_3^{max}=41. All the set of multiquantum transitions are calculated and stored in a 3D matrix with the dimensions ($v_{initial}$,v_{final},T). The temperature values are provided by steps of 100K: T=[100, 200, 300, $\cdots$, 100,000]K.

If users wish to select a lower cutoff parameter (for example the dissociation energy of CO_2 at 5.52eV), then it is simply necessary to find the corresponding $v_{1,2,3}^{max}$ values (36, 64, 22) and trim the coefficient matrix accordingly.

3.6.1 Approximate model for CO_2 dissociation

Since this version does not yet accounts for the excited electronic levels of CO_2 we propose accounting for dissociation processes in a very simplistic fashion: If a transition occurs to a CO_2 level above 5.52eV (lowest dissociation limit of CO_2), then we consider that there is an unit probability that the molecule will dissociate in the next collision. The dissociation rate will then correspond to the sum of the transition rates to the all the levels above the dissociation threshold. This approach is identical to the one discussed in Refs. [14, 12].

3.6.2 Datafiles format

The rate coefficients matrix is proposed in three different formats:

- a MATLAB matrix with the dimensions (v_{ini},v_{fin},1000[9])
- an ASCII file

[9] corresponding to T=[100, 200, 300, $\cdots$, 100,000]K

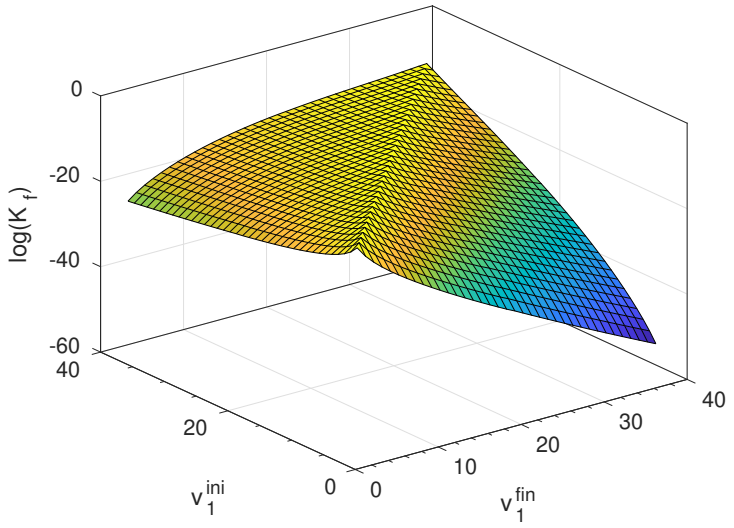

Figure 18: Sample multiquantum rates for v_1 V–T rates at 1000K translational temperature

- a BINARY file. it contains six signed integer numbers corresponding to v_{ini}, v_{fin}, 1000, T_{min}, T_{step}, T_{max}, followed by a sequential writing of the matrix in floating single precision.

The full dataset of rates may be downloaded from the following address: http://esther.tecnico.ulisboa.pt/stellar.html

4 Shortcomings of the Implemented Models

As discussed in the introduction, the STELLAR database has the aim of providing a dataset of "credible" vibrational rates for CO_2, calibrated against experimental data from the literature, or in some cases against more detailed (PES-based) modeling data. This dataset cannot have the ambition to provide an accurate or near-perfect picture of the state-specific physical-chemical processes in CO_2 since it has to sacrifice a great deal of detail in exchange for making the approach tractable with reduced computational costs, and effective scalability allowing the production of a global dataset of rates.

An attempt to identify (at least qualitatively) the overall shortcomings of the approach deployed in STELLAR is provided in this section, in the form of a shortlist. The shortcomings that will be addressed in future updates of the database will firstly be listed, followed by the more underlying shortcomings specific to the model itself.

The shortcomings that will be addressed in future updates of the database are:

- The rates of collision are the same independently of the collisional partner, and assumed to be the same that for the CO_2 collisional partner. This assumption is temporarily used as a matter of convenience, with CO_2 selected as the reference collisional partner, since in most applications of interest the main chemical species in the flow will be CO_2 (not valid for highly diluted gases or highly dissociated gases). This assumption will be reviewed in v_2.5 of the database.
- The current model does not include intermode transitions other than for resonant levels. General intermode transitions may also be calculated resorting to simple adaptations of the FHO model

but it is currently unclear to whether the FHO model may be effectively extrapolated to model intermode transitions other than the ones for which there is experimental data. It is also unclear whether these need to be accounted for, in the sense that resonant transitions might be enough to effectively redistribute level populations between the different modes, with the other rates being low enough that they may be neglected.

- The current model does not account for low-temperature rate increase due to intermolecular attractive forces. This may be accounted for resorting to the Sharma–Brau theory [21] and the corresponding rates summed to the FHO rates (since the former are negligible in the high temperature limit and the latter in the low temperature limit. This is expected to be accounted for in version 3 of the database

- It is very well known that dissociation of CO_2 proceeds from a crossing from the ground electronic state of CO_2 up to an excited electronic state $^3B_2$, followed to a dissociation to the ground states of CO and O. This pathway has an energy jump of 5.52eV as opposed to the 7.42eV for the direct dissociation from the $X^1\Sigma$ state. Future updates of the STELLAR database (v_3) will account for crossings between the $X^1\Sigma$ and $^3B_2$ states, using the Rosen–Zener theory. The transitions for the three *ss*, *be*, and *as* modes of the $^3B_2$ state will then be modeled for the calculated manifold of vibrational levels for this excited state, assuming the same intermolecular potentials than for the $X^1\Sigma$ state (as there is no experimental or modeling data to calibrate this kind of rates.

The more underlying shortcomings are:

- The extrapolation of a PES in its 3 modes limit (*ss*, *be*, *as*) by a representative repulsive and near-dissociation potential, while not as accurate as defining a proper PES near-dissociation potential (which is not carried out in the Ames-1 PES), should provide the correct near-dissociation trends, as compared with the usual extrapolation of polynomial expansions. Past similar approaches for diatomic molecules have provided very accurate results [2]

- The database assumes full separation of the three vibrational modes of CO_2. This means that for example the rate $CO_2(n', m', p') \rightarrow CO_2(n'', m', p')$ will be the same no matter what the m and p quantum numbers are. Billing calculations from Ref. [20] shown that differences from a factor of 5 (at room temperature) down to a factor of 1.5 (at 2000K). Future updates of the approach of this report could include resorting to a more accurate description of the level energies, including the couplings between different vibrational modes. Then it could be investigated whether the corresponding rates (with differing ΔE) could reproduce the differences evidenced in Billing's works.

- Considering an isotropic Morse-like intermolecular potential, and assuming the collision as 1D with the application of a steric factor. Comparisons carried out with the FHO model against PES-based methods show that rates with the same order of magnitude are achieved. However the temperature dependence at low-temperatures is poorly reproduced by the FHO model, and attractive low-temperature effects should be modeled resorting to the Sharma–Brau [21] theory, and added to the rate provided by the FHO theory. Results in the higher temperature limit have a better agreement with PES results, as would be expected in the Landau–Teller limit (increasing $\log(K_f)$ over $T^{-1/3}$). Regarding the scaling of rates to higher vibrational quantum levels, there is not enough PES-based data to provide a meaningful comparison.

- There is no specific accounting of the l_2 bending quantum numbers, and transitions from any $v_2^{l_2}$ levels are assumed to have equivalent rates. Billing calculations from Ref. [22] predict differences ranging from a factor of 5 to one order of magnitude in transitions from the same v_2 level, depending on the l_2 quantum number.

- Influence of rotation is not accounted for. The inclusion of explicit rotational levels in state-to-state models is still in general beyond the computational capabilities of the present, regarding both the production of a dataset of (v, J) rates, and the deployment of such a dataset of kinetic rates for practical computations. Currently only exploratory works regarding atom-diatom and diatom-diatom collisions exist.

- Non Born–Oppeheimer (nBO) effects for the higher quantum levels: High-energy and near-dissociation levels of CO_2 are likely to be affected by these nBO effects, such as for example those evidenced by the increasing presence of perturbations in the higher levels of the CDSD4000 database [23]. No known studies exist on nBO effects for the higher levels of CO_2, therefore it is not possible to quantify the influence of such effects in a global model.

5 Conclusions

Overall we expect these proposed rates to provide a reasonable description of the vibrational excitation processes in CO_2, and all the parameters for the calculation (such as the intermolecular potential) have been carefully checked against available experimental data. Namely:

- The intermolecular potential has been fitted against v_2 V–T quenching rates. This potential shows excellent agreement with a large dataset of quantum transitions (5–4 down to 1–0 v_2 transitions)and is within bounds of experimentally and numerically determined intermolecular potentials.

- The same V–T and V–V–T steric factors than for the v_2 V–T transitions yield v_2/v_3 and v_2/v_1 transition ratios which are within bounds of the ones assumed in the literature.

- v_2 and v_3 V–V–T transitions are accurately reproduced by the same intermolecular parameters, despite the need to adjust the steric factor S_{VT} in some cases

- Near resonant V–V–T transitions are insensitive to the V–V–T S_{VVT} steric factor, considering the semi-empirical correction brough to the FHO theory for modeling these processes. For the sake of simplicty we assume $S_{VVT} = S_{VT}$ for all transitions.

Needless to say, these results supersede by far the previous approaches based on the SSH theory. The FHO theory is capable of providing physically-consistent rates (transition probabilities never exceed one) and scales more accurately to higher quantum numbers.

A limited amount of resonant intermode exchange transitions are also provided, which allow forgoing the Fermi coupling assumption, since many results from the literature lead us to question its systematic application. It is simply better to just calculate the transition rates for each vibrational mode v_1 and v_2 individually without making any a-priori assumptions. It is still left to verify if these exchange rates are sufficient for an realistic energy redistribution among CO_2 different vibrational modes. This will need to be checked in practical applications using the STELLAR database.

Citing this work

This work should be cited as:

M. Lino da Silva, J. Vargas, and J. Loureiro, "*STELLAR CO_2 v_2: A database for vibrationally-specific excitation and dissociation rates for Carbon Dioxide*", Tech. Rep. IST–IPFN TR 06–2018, ESA Contract No. 4000118059/16/NL/KML/fg "Standard Kinetic Models for CO_2 Dissociating Flows", December 2018.

A List of resonant v_1, v_2, v_3 levels

Table 10: Resonant CO_2 levels and corresponding rates

(v_1',v_2',v_3')	(v_1'',v_2'',v_3'')	ΔE_v	Rate
(1,0,0)[a]	(0,2,0)	1.488	Eq. 17
(2,0,0)[a]	(0,4,0)	10.623	Eq. 17
(3,0,0)[a]	(0,6,0)	27.663	Eq. 18
(0,0,2)	(0,7,0)	3.774	Eq. 17
(4,0,0)[a]	(0,8,0)	52.862	Eq. 18
(5,0,0)[a]	(0,10,0)	86.478	Eq. 18
(7,0,0)	(0,0,4)	50.731	Eq. 18
(0,17,0)	(0,0,5)	98.446	Eq. 18
(0,23,0)	(12,0,0)	99.923	Eq. 18
(13,0,0)	(0,25,0)	8.870	Eq. 17
(14,0,0)	(0,0,8)	46.905	Eq. 18
(0,0,8)	(0,27,0)	81.425	Eq. 18
(0,30,0)	(0, 0,9)	21.620	Eq. 17
(0,0,10)	(0,33,0)	15.251	Eq. 17
(18,0,0)	(0,34,0)	30.780	Eq. 18
(0,0,11)	(0,36,0)	81.410	Eq. 18
(0,39,0)	(21,0,0)	99.058	Eq. 18
(22,0,0)	(0,41,0)	76.700	Eq. 18
(0,46,0)	(25,0,0)	51.866	Eq. 18
(0,0,21)	(0,61,0)	64.683	Eq. 18
(0,61,0)	(34,0,0)	68.475	Eq. 18
(0,0,22)	(0,63,0)	4.724	Eq. 17
(0,0,23)	(0,65,0)	2.371	Eq. 17
(37,0,0)	(0,66,0)	62.628	Eq. 18
(0,0,24)	(0,67,0)	58.591	Eq. 18
(0,69,0)	(39,0,0)	49.808	Eq. 18
(0,0,26)	(40,0,0)	83.708	Eq. 18
(41,0,0)	(0,0,27)	4.882	Eq. 17
(42,0,0)	(0,0,28)	39.485	Eq. 18
(43,0,0)	(0,0,29)	18.733	Eq. 17
(0,0,30)	(44,0,0)	58.804	Eq. 18
(0,0,31)	(0,78,0)	0.395	Eq. 17
(0,0,37)	(0,84,0)	84.119	Eq. 18
(0,0,39)	(0,85,0)	6.090	Eq. 17
(0,0,41)	(50,0,0)	20.508	Eq. 17

[a]: Fermi resonances

References

[1] X. Huang, D. W. Schwenke, S. A. Tashkun, and T. J. Lee, "An Isotopic-Independent Highly Accurate Potential Energy Surface for CO_2 Isotopologues and an Initial $^{12}C^{16}O_2$ Infrared Line List", *J. Chem. Phys.*, Vol. 136, 2012, p. 124311

[2] M. Lino da Silva, V. Guerra, J. Loureiro, and P.A. Sá, "Vibrational Distributions in N_2 With an Improved Calculation of Energy Levels Using the RKR Method", *Chem. Phys.*, Vol. 348, No. 1–3, 2008, pp. 187–194.

[3] W. Quapp, B. P. Winnewisser "What You Thought you Already knew about the Bending Motion of Triatomic Molecules", *Journal of Mathematical Chemistry*, Vol. 14, 1993, pp. 259–285.

[4] T. W. Chen, "Turning Point Approximation and Application to Nonlinear Oscillators", *American Journal of Physics*, Vol. 48, No. 4, 1980, pp.292–296.

[5] H. Khun, H.-D. Försterling, and D. H. Waldeck, *"Principles of Physical Chemistry, 2nd Edition"*, Wiley, 2009, ISBN 978-0-470-08964-4.

[6] D. Rapp and T. Kassal, "The Theory of Vibrational Energy Transfer Between Simple Molecules in Nonreactive Collisions", *Chemical Reviews*, Vol. 69, 1969, pp. 61–102.

[7] J. Yardley, *"Introduction to Molecular Energy Transfer"*, 1st. Edition, 1980, Academic Press

[8] E. H. Kerner, "Note on the Forced and Damped Oscillations in Quantum Mechanics", *Canadian Journal of Physics*, Vol. 36, No. 3, 1958, pp. 371–377.

[9] C. E. Treanor, "Vibrational Energy Transfer in High-Energy Collisions", *Journal of Chemical Physics*, Vol. 43, No. 2, 1965, pp. 532–538.

[10] A. Zelechow, D. Rapp, and T. E. Sharp, "Vibrational-Vibrational-Translational Energy Transfer Between Two Diatomic Molecules", *Journal of Chemical Physics*, Vol. 49, No. 1, 1968, pp. 286–299.

[11] T. L. Cotrell, and N. Ream, "Transition Probability in Molecular Encounters Part I. The Evaluation of Perturbation Integrals", *Transactions of the Faraday Society*, Vol. 51, No. 1, 1955, pp. 159–171.

[12] M. Lino da Silva, V. Guerra, and J. Loureiro, "State-Resolved Dissociation Rates for Extremely Nonequilibrium Atmospheric Entries", *J. Thermophys. Heat Transf.* Vol. 21, No. 1, 2007, pp. 40–49.

[13] E. E. Nikitin, and A. I. Osipov, "Vibrational Relaxation in Gases", *Kinetic and Catalysis*, Vol. 4, VINITI, All-Union Institute of Scientific and Technical Information, Moscow, 1977, Chap. 2.

[14] I. V. Adamovich, S. O. Macheret, J. W. Rich, and C. E. Treanor, "Vibrational Relaxation and Dissociation Behind Shock Waves Part 1: Kinetic Rate Models", *AIAA Journal*, Vol. 33, No. 6, 1995, pp. 1064–1069.

[15] I. V. Adamovich, S. O. Macheret, J. W. Rich, and C. E. Treanor, "Vibrational Relaxation Behind Shock Waves Part II: Master Equation Modeling" *AIAA Journal*, Vol. 33, No. 6, 1995, pp. 1070–1075.

[16] I. V. Adamovich, S. O. Macheret, J. W. Rich, and C. E. Treanor, "Vibrational Energy Transfer Rates Using a Forced Harmonic Oscillator Model", *Journal of Thermophysics and Heat Transfer*, Vol. 12, No. 1, 1998, pp. 57–65.

[17] I. V. Adamovich, and J. W. Rich, "Three-Dimensional Nonperturbative Analytic Model of Vibrationally Energy Transfer in Atom-Molecule Collisions", *Journal of Chemical Physics*, Vol. 109, No. 18, 1998, pp. 7711–7724.

[18] S. O. Macheret, and I. V. Adamovich, "Semiclassical Modeling of State-Specific Dissociation Rates in Diatomic Gases", *Journal of Chemical Physics*, Vol. 113, No. 17, 2000, pp. 7351–7361.

[19] A. Chedin, "The Carbon Dioxide Molecule: Potential, Spectroscopic, and Molecular Constants From its Infrared Spectrum, *J. Mol. Spectrosc.*, Vol. 76, No. 1–3, 1979, pp. 430-491.

[20] G. D. Billing, "Semiclassical Calculation of Energy Transfer in Polyatomic Molecules. I. The CO_2–N_2 System", *J. Chem. Phys.*, Vol. 41, No. 1–2, 1979, pp. 11–20

[21] R. D. Sharma, and C. A. Brau, "Energy Transfer in Near-Resonant Molecular Collisions Due to Long-Range Forces With Application to Transfer of Vibrational Energy from ν_3 Mode of CO_2 to N_2", *Journal of Chemical Physics*, Vol. 50, No. 2, 1969, pp. 924–930.

[22] G. D. Billing, "Semiclassical Calculation of Energy Transfer in Polyatomic Molecules. VI. On the Theory for Linear Triatomic Molecules", *J. Chem. Phys.*, Vol. 61, No. 3, 1981, pp. 415–430

[23] J. F. Vargas, B. Lopez, M. Panesi, and M. Lino da Silva, "Refitting of Detailed CO_2 IR Databases to Vibrationally Specific Databases Tailored for Aerothermodynamic Flows", *AIAA Paper 2018–4177*, 2018 Joint Thermophysics and Heat Transfer Conference, AIAA AVIATION Forum, Atlanta, Georgia, 25–29 June 2018.

[24] M. Lino da Silva, J. Loureiro, and V. Guerra, "A Multiquantum Dataset for Vibrational Excitation and Dissociation in High-Temperature O_2–O_2 Collisions", *Chem. Phys. Lett.*, Vol. 531, 2012, pp. 28-33.

[25] V. B. Leonas, "Studies of Short-Range Intermolecular Forces", *Sov. Phys. Usp.*, Vol. 15, No. 3, 1972, pp. 266–281

[26] S. Bock, E. Bich, and E. Vogel. "A New Intermolecular Potential Energy Surface for Carbon Dioxide From Ab-Initio Calculations", *Chem. Phys.*, Vol. 257, No. 2–3, 2000, pp. 147–156.

[27] J. Blauer, and G. Nickerson, "A Survey of Vibrational Relaxation Rate Data for Processes Important to CO_2-N_2-H_2O Infrared Plume Radiation", *AIAA Paper 1974-536*, 7th Fluid and PlasmaDynamics Conference, 1974.

[28] S. A. Losev, "Kinetics of Vibrational Energy Exchange in Carbon Dioxide Gas and its Mixtures with Other Gases", *Combust. Explos. Shock Waves (USSR)* No. 2, 1976, pp. 141–155.

[29] A. S. Biryukov, V. K. Konyukhov, A. I. Lukovnikov, and R. I. Serikov. "Relaxation of the Vibrational Energy of the (00^01) Level of the CO_2 Molecule", *Zh. Eksp. Teor. Fiz.*, Vol. 66, 1974, pp. 1248–1257.

[30] G. C. Schatz, and M. J. Redmon, "A Quasiclassical Trajectory Study of Collisional Excitation in $O(^3P)$+CO_2", *Chem. Phys.*, Vol. 58, 1981, pp. 195–201.

[31] D. C. Clary, "Quantum Study of Vibrational Excitation in the Three-Dimensional Collisions Of CO_2 With Rare Gas Atoms", *J. Chem. Phys.*, Vol. 75, No. 209, 1911, pp. 209–2019.

[32] J. O. Chu, G. W. Flynn, and R. E. Weston Jr., "Spectral Distribution of CO_2 Vibrational States Produced by Collisions With Fast Hydrogen Atoms From Laser Photolysis of HBr", *J. Chem. Phys.*, Vol. 78, No. 6, 1983, pp. 2990–2997.

[33] R. M. Siddles, G. J. Wilson, and C. J. S. M. Simpson, "The Vibrational Deactivation of the ($00^0 1$) and ($01^1 0$) Modes of CO_2 Measured Down to 140 K", *Chem. Phys.*, Vol. 189, 1994, pp. 779–791.

[34] N. Mullaney Harvey, "A Quantum Mechanical Investigation of Vibrational Energy Transfer in $O(^3P)$+CO_2 Collisions", *Chem. Phys. Lett.*, Vol. 88, No. 6, 1982, pp. 553–558.

[35] M. Lopez–Puertas, and F. W. Taylor, "Non-LTE Radiative Transfer in the Atmosphere", Vol. 3. *World Scientific*, 2001.

[36] M. P. de Lara-Castells, M. I. HernÃ¡ndez, G. Delgado-Barrio, P. Villarreal, and M. López-Puertas, "Vibrational Quenching of CO2(010) by Collisions with $O(^3P)$ at Thermal Energies: A Quantum-Mechanical Study", *J. Chem. Phys.*, Vol. 124, No. 16, 2006, p. 164302.

[37] K. J. Castle, L. A. Black, M. W. Simione, and J. A. Dodd"Vibrational Relaxation of $CO_2(v_2)$ by $O(^3P)$ in the 142–490 K Temperature Range", *J. Geophys. Res.*, Vol. 117, No. A04310, 6 pp.

[38] R. E. Center, "Vibrational Relaxation of CO_2 by O Atoms"*J. Chem. Phys.*, Vol. 59, No. 7, 1973, pp. 3523–3527.

[39] C. B. Moore, R. E. Wood, B.–L. Hu, and J. T. Yardley, "Vibrational Energy Transfer in CO_2 Lasers", *J. Chem. Phys.*, Vol. 46, No. 11, 1967, pp. 4222–4231.

[40] A. Fridman, *"Plasma Chemistry"*, 2008, Cambridge: Cambridge University Press.

[41] E. V. Kustova, E. A. Nagnibeda, and I. Armenise, "Vibrational-Chemical Kinetics in Mars Entry Problems", *Open Plasma Phys. J.*, Vol. 7, Suppl 1: M5, 2014, pp. 76-87.

[42] I. Armenise, I.,and E. Kustova, "Mechanisms of Coupled Vibrational Relaxation and Dissociation in Carbon Dioxide", *J. Phys. Chem. A*, Vol. 122, No. 23, 2018, pp. 5107–5120.

[43] T. Kozák, and A. Bogaerts, "Splitting of CO_2 by Vibrational Excitation in Non-Equilibrium Plasmas: A Reaction Kinetics Model", *Plasma Sources Sci. Technol.*, Vol. 23, No. 4, 2014, No. 045004.

[44] L. V. Eckermann, C. J. Flynn, and K. J. Castle, "Vibrational Relaxation in CO_2 ($10^0 0$)–CO_2 Collisions" *ACS Earth and Space Chemistry*, 2018, Article ASAP.

[45] W. A. Rosser, E. Hoag, and E. T. Gerry, "Relaxation of Excess Populations in the Lower Laser Level $CO_2(100)$", *J. Chem. Phys.*, Vol. 57, No. 10, 1972, pp. 4153–4164.

[46] D. C. Allen, T. Scragg, and C. J. S. M. Simpson, "Low Temperature Fluorescence Studies of the Deactivation of the Bend-Stretch Manifold of CO_2, *Chem. Phys.*, Vol. 51, No. 3, 1980, pp. 279–298.

[47] G. Millot, and C. Roche, "State-to-State Vibrational and Rotational Energy Transfer in CO_2 Gas from Time-Resolved Raman-Infrared Double Resonance Experiments, "*Journal of Raman Spectroscopy*, Vol. 29, 1998, pp. 313–320.

[48] V. Joly, and A. Roblin, "Vibrational Relaxation of $CO_2(m,n^1,p)$ in a CO_2–N_2 Mixture. Part 2: Application to a One-Dimensional Problem", *Aerospace Sci. Tech.*, No. 4, 1999, pp. 229–238.

[49] J. Finzi and C. B. Moore, "Relaxation of $CO_2(10^0 1)$, $CO_2(02^0 1)$, and $N_2O(10^0 1)$ Vibrational Levels by Nearresonant V→V Energy Transfer", *J. Chem. Phys.*, Vol. 63, No. 6, 1975, pp. 2285-2288.

[50] Svehla, R. A., "Estimated Viscosities and Thermal Conductivities of Gases at High Temperatures", *NASA Tech. Rep.* R–132, 1962.

[51] L. Landau and E. Teller, in: *L. D. Landau. Collection of Papers [in Russian]*, Vol. 1, Moscow (1969), pp. 181–188.

[52] V. V. Nevdakh, L. N. Orlov, and N. S. Leshenyuk, "Temperature Dependence of the Vibrational Relaxation Rate Constants of CO_2 (00^01) In Binary Mixtures", *J. Appl. Spectrosc.*, Vol. 70, No. 2, 2003, pp. 276–284.

[53] T. G. Kreutz, J. A. O'Neill, and G. W. Flynn, "Diode Laser Absorption Probe of Vibration-Vibration Energy Transfer in CO_2", *J . Phys. Chem.*, Vol. 91, 1987, pp. 5540–5543.

[54] M. D. Thomason, *Ph.D. Thesis*, University of Virginia, Los Alamos National Laboratory, LA9420-T, 1982.

[55] L. Taylor, and S. Bitterman, "Survey of Vibrational Relaxation Data for Processes Important in the CO_2–N_2 Laser System", *Rev. Mod. Phys.*, Vol. 41, No. 1, 1969, pp. 26–47.

[56] W. A. Rosser Jr, A. D. Wood, and E. T. Gerry, "Deactivation of Vibrationally Excited Carbon Dioxide (ν_3) by Collisions With Carbon Dioxide or With Nitrogen", *J. Chem. Phys.*, Vol. 50, No. 11, 1969, pp. 4996–5008.

[57] N. S. Leshenyuk, V. V. Nevdakh, and L. N. Orlo, "Vibrational Relaxation in a CO_2–N_2 Mixture", *Journal of Applied Spectroscopy*, Vol. 34, No. 6, 1981, pp. 605–609.

[58] D. J. Miller, and R. C. Millikan, "Vibration-Vibration Energy Exchange Between Carbon Monoxide and Carbon Dioxide", *Chem. Phys.*, Vol. 6, No. 2, 1974, pp. 317–324.